

# Supporting Information For: The Significance of the Amorphous Potential Energy Landscape for Dictating Glassy Dynamics and Driving Solid-State Crystallisation

Michael T. Ruggiero,<sup>†</sup> Marcin Krynski,<sup>‡</sup> Eric Ofosu Kissi,<sup>¶</sup> Juraj Sibik,<sup>†,⊥</sup> Daniel  
Markl,<sup>†</sup> Nicholas Y. Tan,<sup>†</sup> Denis Arslanov,<sup>§, #</sup> Wim van der Zande,<sup>§, @</sup> Britta  
Redlich,<sup>§</sup> Timothy M. Korter,<sup>||</sup> Holger Grohganz,<sup>¶</sup> Korbinian Lobmann,<sup>¶</sup> Thomas  
Rades,<sup>¶</sup> Stephen R. Elliott,<sup>‡</sup> and J. Axel Zeitler<sup>\*, †</sup>

<sup>†</sup>*Department of Chemical Engineering and Biotechnology, University of Cambridge,  
Philippa Fawcett Drive, Cambridge, CB3 0AS, United Kingdom*

<sup>‡</sup>*Department of Chemistry, University of Cambridge, Lensfield Road, Cambridge, CB2  
1EW, United Kingdom*

<sup>¶</sup>*Department of Pharmacy, University of Copenhagen, Universitetsparken 2, 2100  
Copenhagen, Denmark*

<sup>§</sup>*Radboud University, Institute for Molecules and Materials, FELIX Laboratory,  
Toernooiveld 7c, 6252 ED Nijmegen, The Netherlands*

<sup>||</sup>*Department of Chemistry, Syracuse University, Syracuse, New York, 13244, United States  
of America*

<sup>⊥</sup>*Present address: F. Hoffmann-La Roche AG, Konzern-Hauptsitz, Basel, Switzerland*

<sup>#</sup>*Present address: ASM Laser Separation International, Beuningen, The Netherlands*

<sup>@</sup>*Present address: ASML, Veldhoven, The Netherlands*

E-mail: jaz22@cam.ac.uk

Phone: +44 (0) 1223 334783

## **Terahertz Time-Domain Spectroscopy**

Amorphous sorbitol was prepared by melting as-received sorbitol (99%, Sigma Aldrich, Poole, UK) between two 13 mm diameter and 2 mm thick z-cut quartz windows on a standard laboratory hot plate. The samples were loaded into a Janis cryostat, along with a corresponding set of two z-cut quartz windows to act as a standard blank. Data were acquired at 20 K intervals through the use of liquid nitrogen coolant, while the temperature was maintained using a Lakeshore 330 temperature controller and heating unit.

Terahertz time-domain spectra were acquired on a commercial TeraView Terapulse 4000 spectrometer. A total of 4000 waveforms for both the sample and blank were acquired at each temperature. Terahertz transmission spectra were obtained through the Fourier transform of the time-domain waveform, and the terahertz absorption spectra were calculated by taking a ratio of the sample and blank data sets.

## **Fourier-Transform Infrared Spectroscopy**

Amorphous sorbitol was prepared by melting as received sorbitol (99%, Sigma Aldrich, Poole, UK) between two sapphire windows. The sample was then loaded into a Specac variable temperature cell holder (Slough, UK) which contained NaCl windows. The FTIR spectra were acquired on a ThermoFisher Nicolet spectrometer that was continuously purged with nitrogen gas. Spectra were acquired in 5 K intervals through the use of liquid-nitrogen coolant.

## **Dynamical Mechanical Analysis**

Melt-quenched glassy sorbitol was loaded into a powder pocket sample holder (for non-self supporting materials), and the sample was fixed into a dual cantilever clamp of a DMA Q800 (TA Instruments- Waters LLC, New Castle, DE, USA). The storage modulus was determined by deforming the sample in an oscillatory manner at a frequency of 1 Hz and

an amplitude of  $20.00\ \mu\text{m}$ , while heating linearly at  $3\ \text{K}\ \text{min}^{-1}$  from 150 to 310 K. From the storage modulus, the onset temperatures of the  $\alpha$ - and  $\beta$ -relaxations were determined.

## Free-electron Laser Experiments

**FLARE** The Free-electron Laser for Advanced spectroscopy and high-Resolution Experiments (FLARE) is a novel, narrow-band, terahertz free-electron laser system situated at the FELIX Laboratory, Radboud University in Nijmegen, which can generate high powered pulsed radiation at frequencies between 200 GHz and 3 THz.

In the pump-probe operational mode, the FLARE output comprises of  $10\ \mu\text{s}$  macro-pulses at a repetition rate of 10 Hz, which themselves contain micro-pulse trains (10 of 100 ps each) at a 3 GHz repetition rate. The average power output at the diagnostic station where experiments are performed is approximately 200 mW when the output frequency is around 1 THz, giving a micropulse power of  $\approx 66\ \text{kW}$  corresponding to a power density of  $3\ \text{MW}\ \text{cm}^{-2}$  when focused with a  $f/6$  parabolic mirror. The focal length of the mirror used was 7 inches and the spot size at the focal point was approximately 3 mm (Figure S1).

**Samples** Carbamazepine and indomethacin were purchased from Sigma Aldrich (99%, Poole, UK) and used without further purification. Thin film amorphous samples were prepared by melting the solid samples directly on a  $13\ \text{mm} \times 2\ \text{mm}$  fused silica window placed within the copper sample cell used for cryogenic measurements. For fully sandwiched samples, a second silica window was placed on top of the melt and the sample holder was screwed onto a copper sample holder before quench cooling with liquid nitrogen. Alternatively, samples were melted on a piece of aluminium foil and quench cooled in liquid nitrogen before being ground to a fine powder with mortar and pestle. Free standing pellets were prepared by compressing the powder into thin flat faced disks of thickness between 1 and 2 mm.

**Sample temperature control** A Specac variable temperature cell holder (Slough, UK) was used to control the temperature of the sample pellets during exposure to FLARE. Sam-

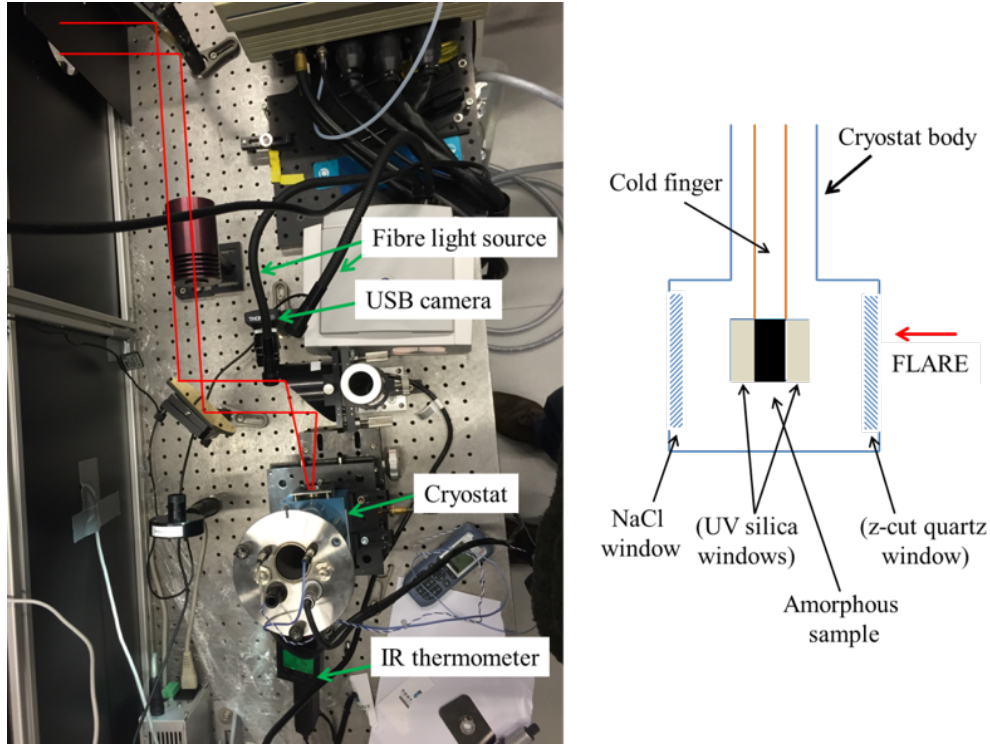


**Figure S1:** Image of experimental setup (left). Red lines indicate beam path of FLARE. Schematic of cryostat showing positions of all windows and the sample (right). Windows named in brackets are not always present in all experimental runs.

ples of the amorphous solids were mounted directly onto the copper sample holder. A NaCl window, which is transparent to infrared (IR) radiation but not to terahertz radiation, was always fixed to the backside of the cell holder to prevent the FLARE beam from interfering with the reading of the bulk sample temperature using an IR thermometer. A z-cut quartz window was occasionally fixed to the side of the cell holder facing the terahertz beam either to reduce the incident FLARE power on the sample or to seal the cryostat so the sample could be kept under vacuum. For experiments with active cooling, the cell holder was kept under vacuum and cooled with liquid nitrogen. The temperature of the cell holder was raised and monitored by an accompanying Specac temperature controller.

In order to accurately monitor the temperature on the sample and quantify the possible heating effects due to the incident terahertz beam, an Optris LS LT IR thermometer (Berlin, Germany) with a temperature range of 238 – 1173 K, accuracy of  $\pm 0.75\%$  and response time

of 150 ms was positioned on the opposing side of the cell holder as the terahertz beam and was focused onto the sample. The focus of the IR thermometer was adjusted to coincide with the terahertz beam spot.

**Further characterisation** A Thorlabs DCC1545M-GL greyscale camera (Munich, Germany) was positioned in front of the sample so that visual changes in the sample appearance could be monitored.

Sample characterisation was performed using a Menlo TERA OSCAT high-speed terahertz spectrometer (Menlo Systems GmbH, Martinsried, Germany) under nitrogen purge.

### *ab initio* Molecular Dynamics (AIMD)

**CP2K** The open-source CP2K software package<sup>1,2</sup> was used to perform AIMD simulations. Ten sorbitol molecules (260 atoms in total) were used for the simulations, which were performed within a cubic simulation box with periodic boundary conditions. The AIMD technique is a fully first-principles density functional theory (DFT) method, and, as such, all of the electrons were treated quantum mechanically using the Perdew-Burke-Ernzerhof (PBE) density functional<sup>3</sup> and the double- $\zeta$  DZVP basis set<sup>4</sup> and Goedecker-Teter-Hutter (GTH) pseudopotentials.<sup>5</sup> London dispersion forces were calculated using the D3 method of Grimme.<sup>6,7</sup> All simulations utilised a Nosé-Hoover chain thermostat to maintain temperature.<sup>8</sup> Isothermal-isobaric ensemble (NPT) simulations utilised an extended Nosé-Hoover barostat as developed by Martyna *et al.*<sup>9,10</sup>

The amorphous structures were generated by quenching a gas-phase system at atmospheric pressure at various temperatures with NPT simulations. The procedure was performed at 50 K increments from 800 K through 50 K, until the density was satisfactorily converged ( $\approx 10 - 15$  ps). The resulting solid structures were then treated by 30 ps NVT simulations, which were performed in order to determine the vibrational dynamics of the system. A 1 fs time-step was used, and the vibrational spectra were determined via the

Fourier transform of the dipole moment autocorrelation function,<sup>11,12</sup> with post-processing performed using the TRAVIS software package.<sup>13</sup>

**VASP** The Vienna Ab-initio Simulation Package (VASP),<sup>14-17</sup> which utilised a plane wave basis, was also used for AIMD simulations. The generalised gradient approximation PBE density functional<sup>3</sup> was used for both the exchange and correlation energies. The full potential projector augmented plane-wave approach was used to describe the electronic structure of the solids.<sup>18</sup> The kinetic energy was controlled using a Nosé-Hoover chain thermostat.<sup>8</sup> Reciprocal space sampling in the first Brillouin zone was performed using a Monkhorst-Pack grid.<sup>19</sup> The cut-off energy for the plane-wave basis was set to 450 eV. All calculations were carried out under periodic boundary conditions for 10 sorbitol molecules (260 atoms in total). Amorphous sorbitol was obtained using a melt-and-quench method, starting from atomic configurations generated using Kinetic Monte Carlo simulations. To ensure random distribution of molecules inside a cubic box, the initial configuration was melted at 800 K for 10 ps then quenched to 400 K, with cooling rate of 20K ps<sup>-1</sup> where it was equilibrated for another 10 ps. Next, every 20 K starting from 400 K, 5 ps of AIMD simulations was carried to obtain the data then followed by 5 ps of AIMD when the temperature was decreased with 4 K ps<sup>-1</sup> rate and another 5 ps AIMD for equilibration at the target temperature.

Video of the crystallisation process of indomethacin and carbamazepine while exposed to FLARE is available as an electronic supporting information file.

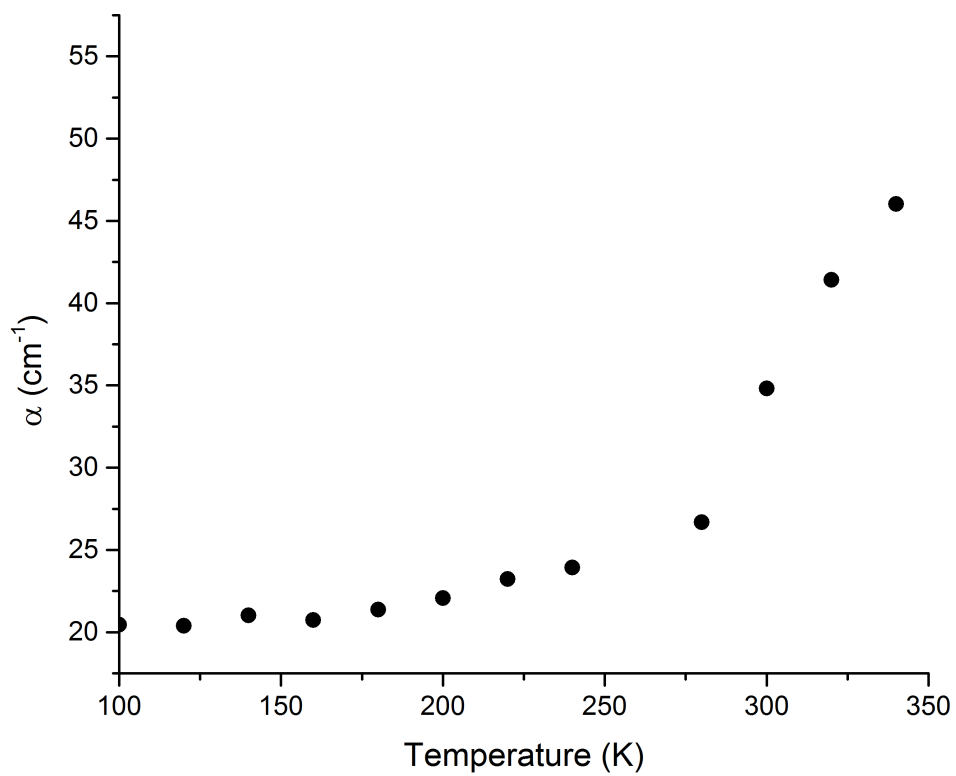


**Figure S2:** Temperature-dependent absorption coefficient at 1 THz of amorphous sorbitol

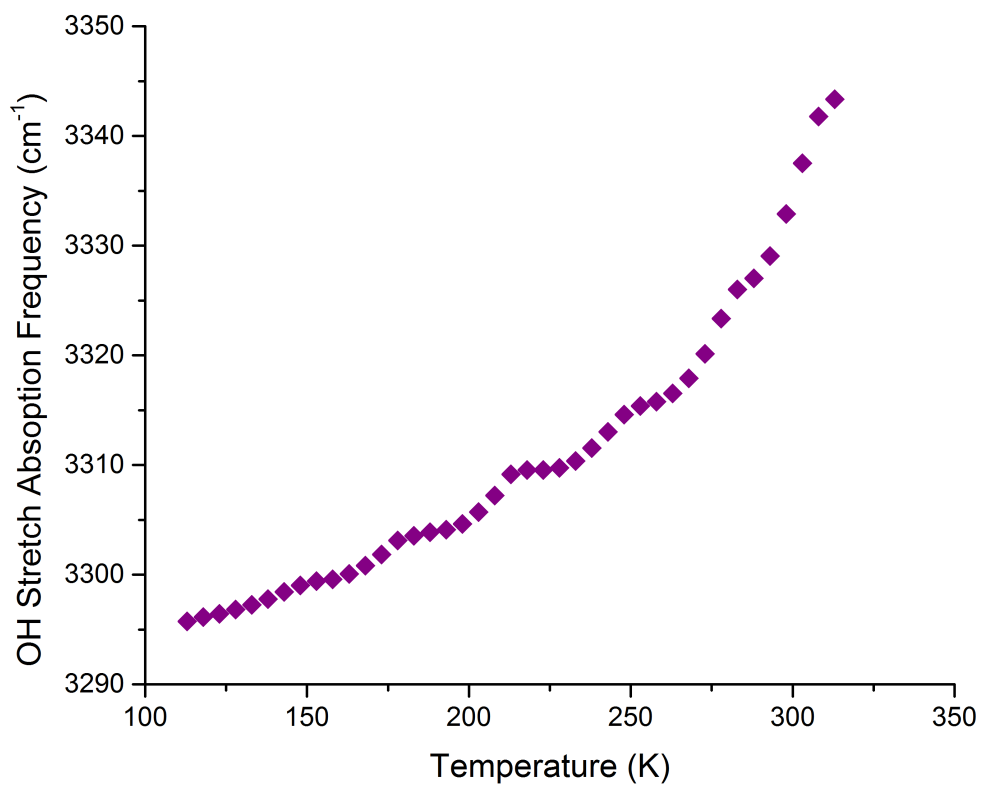


**Figure S3:** Temperature-dependent OH-stretch centre frequency of amorphous sorbitol

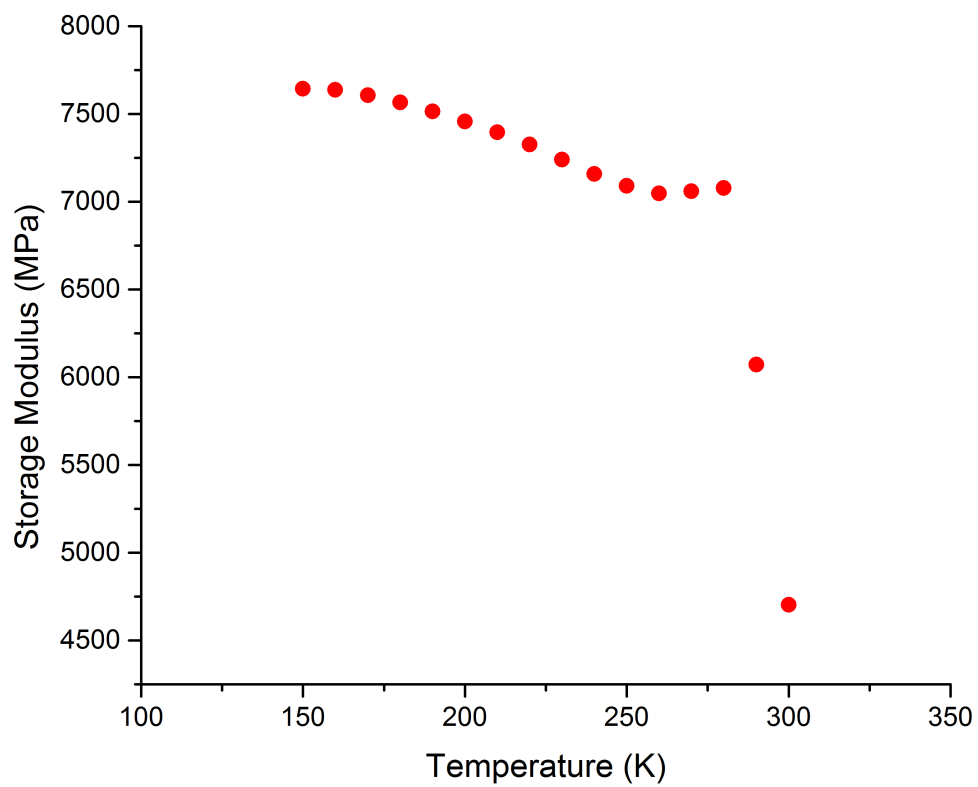


Figure S4: Temperature dependent storage modulus of amorphous sorbitol

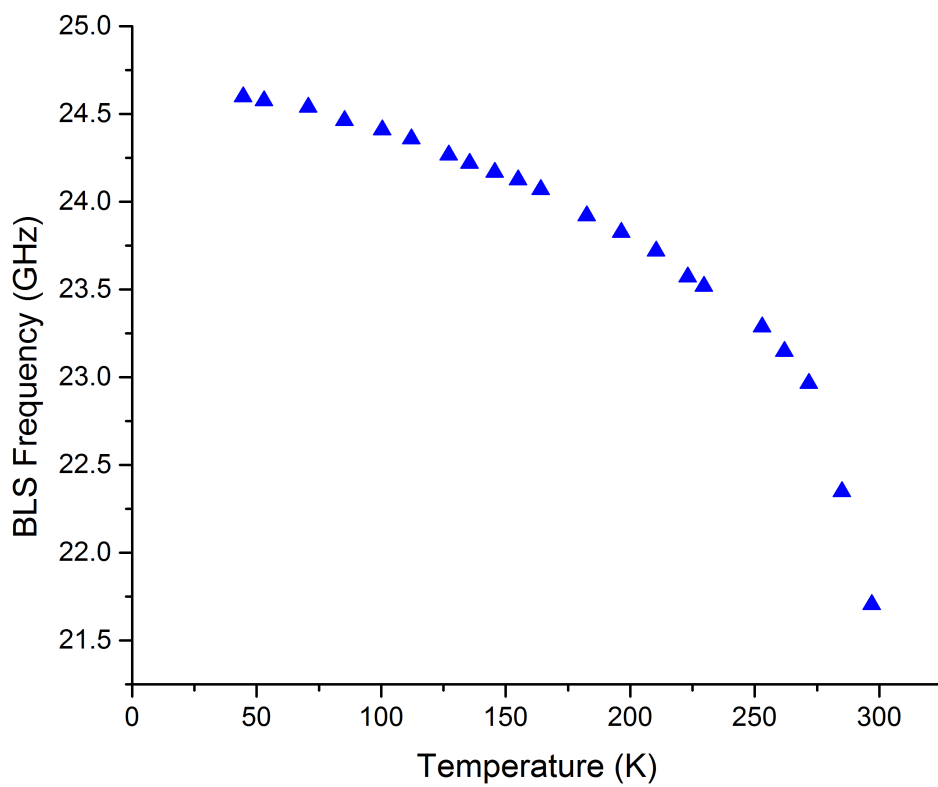
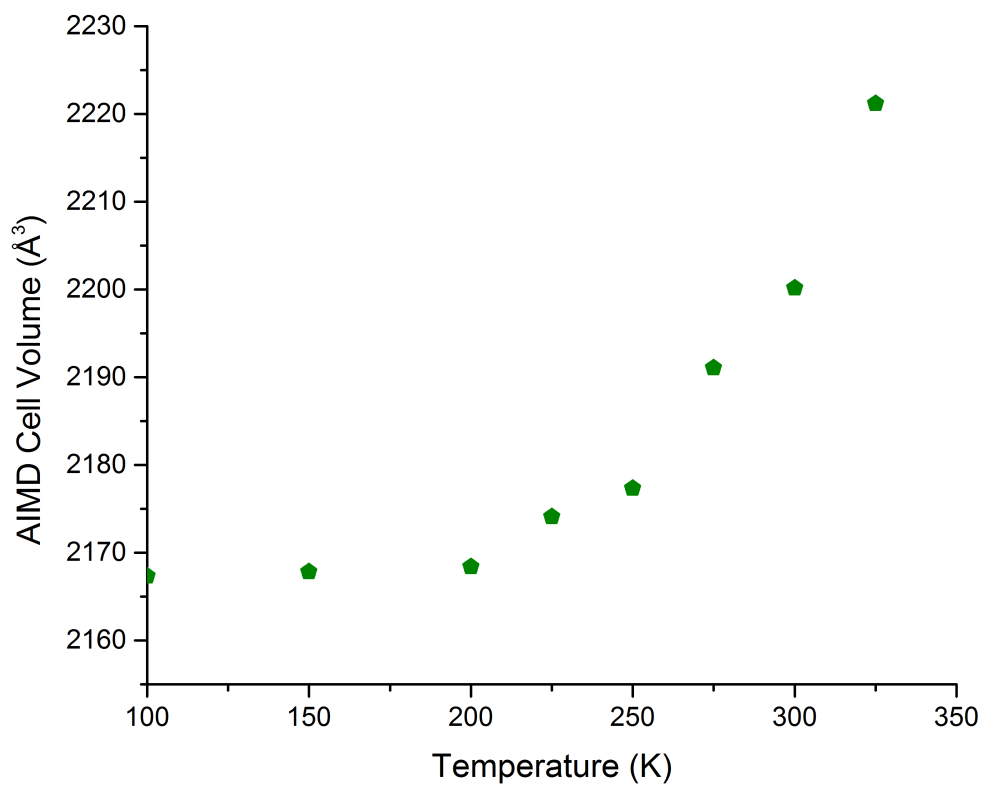


Figure S5: Temperature-dependent BLS scattering peak of amorphous sorbitol digitised from Ruta et. al.<sup>20</sup>



**Figure S6:** AIMD-determined volume of a 10-molecule model of sorbitol in a simulation cell under NPT conditions (standard pressure).

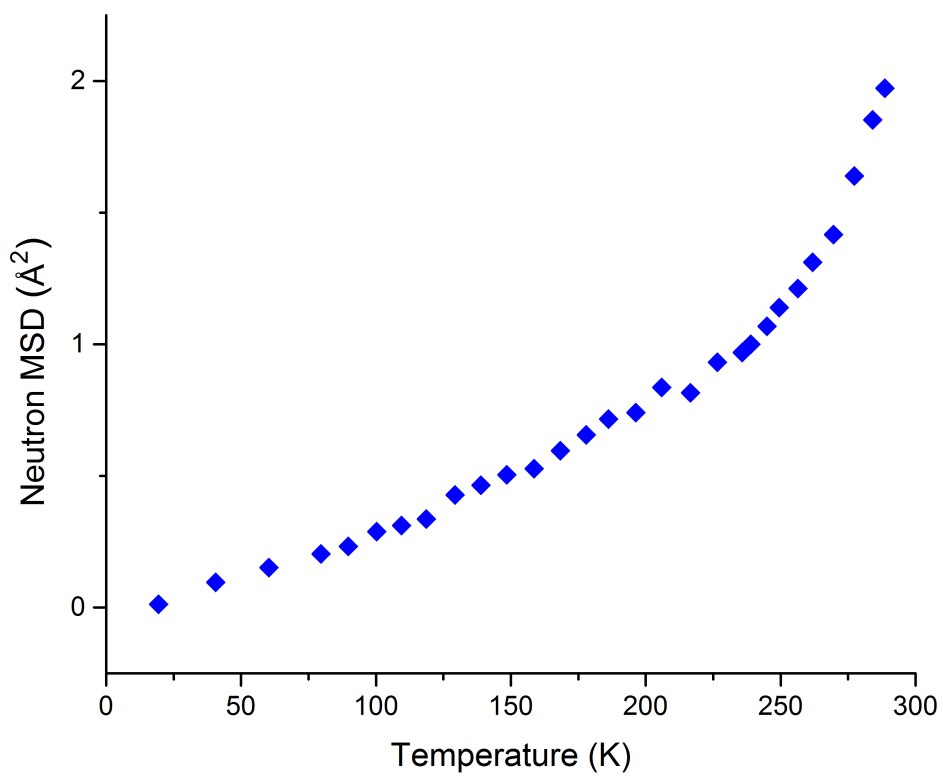


Figure S7: Temperature-dependent neutron-scattering determined mean-squared displacement (MSD) of amorphous OTP digitised from.<sup>21</sup>

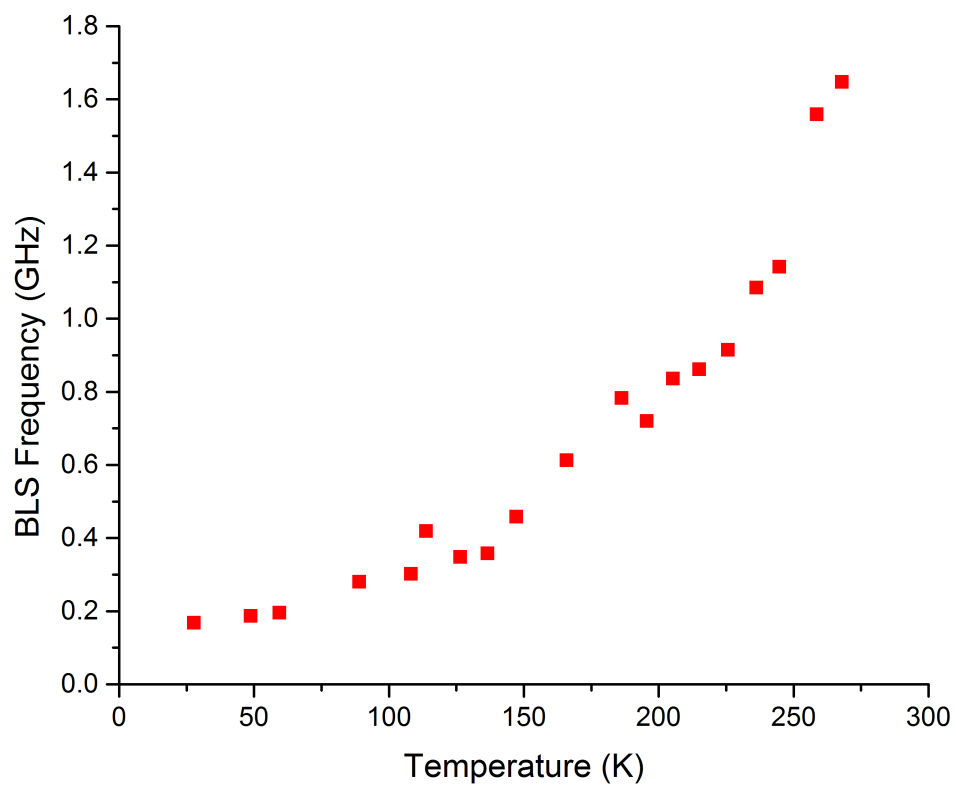


Figure S8: Temperature-dependent BLS scattering peak of amorphous OTP digitised from.<sup>22</sup>

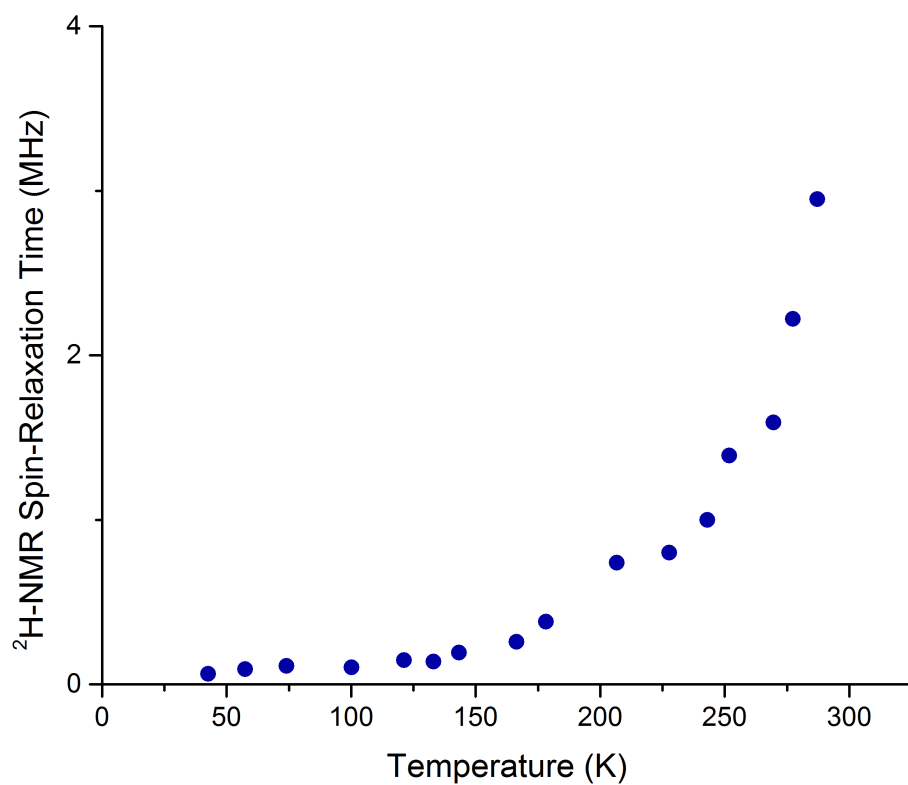


Figure S9: Temperature-dependent  $^2\text{H-NMR}$  spin-lattice relaxation of amorphous OTP digitised from.<sup>23</sup>

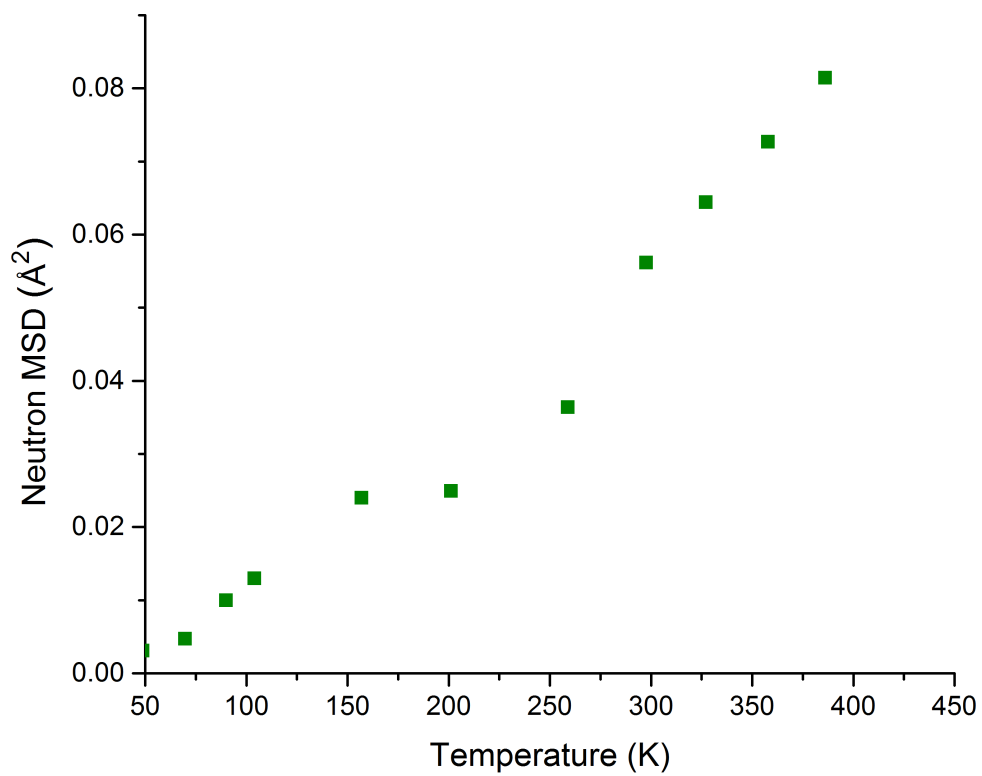


Figure S10: Temperature-dependent neutron-scattering determined mean-squared displacement (MSD) of amorphous PMMA digitised from.<sup>24</sup>

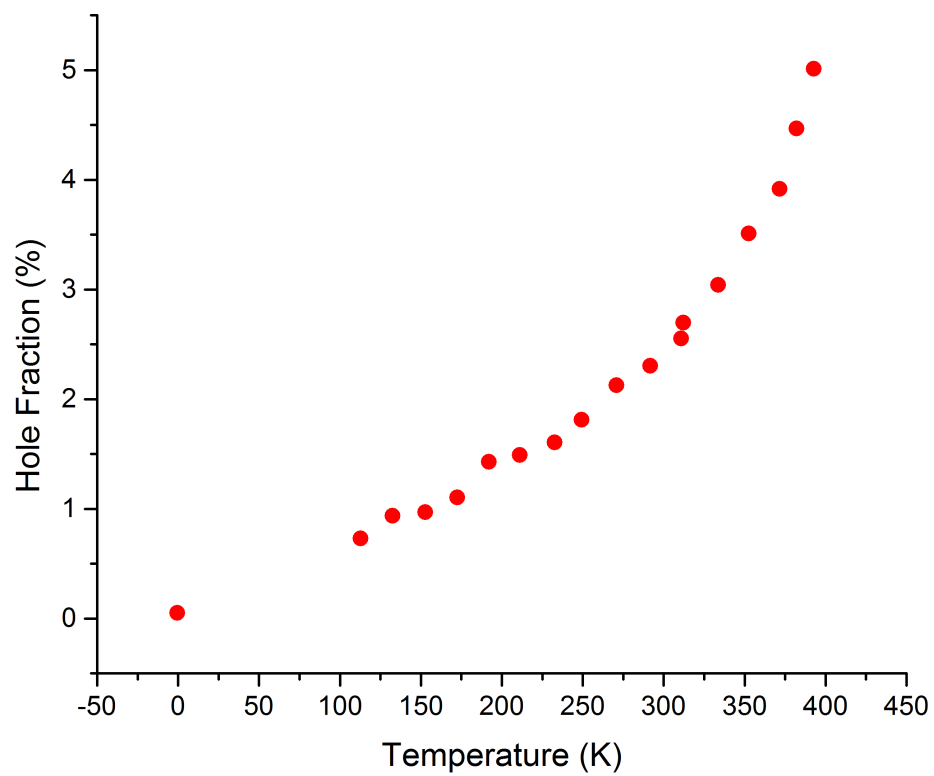


Figure S11: Temperature-dependent positron spectroscopy (PS) determined percent hole fraction of amorphous PMMA digitised from.<sup>25</sup>

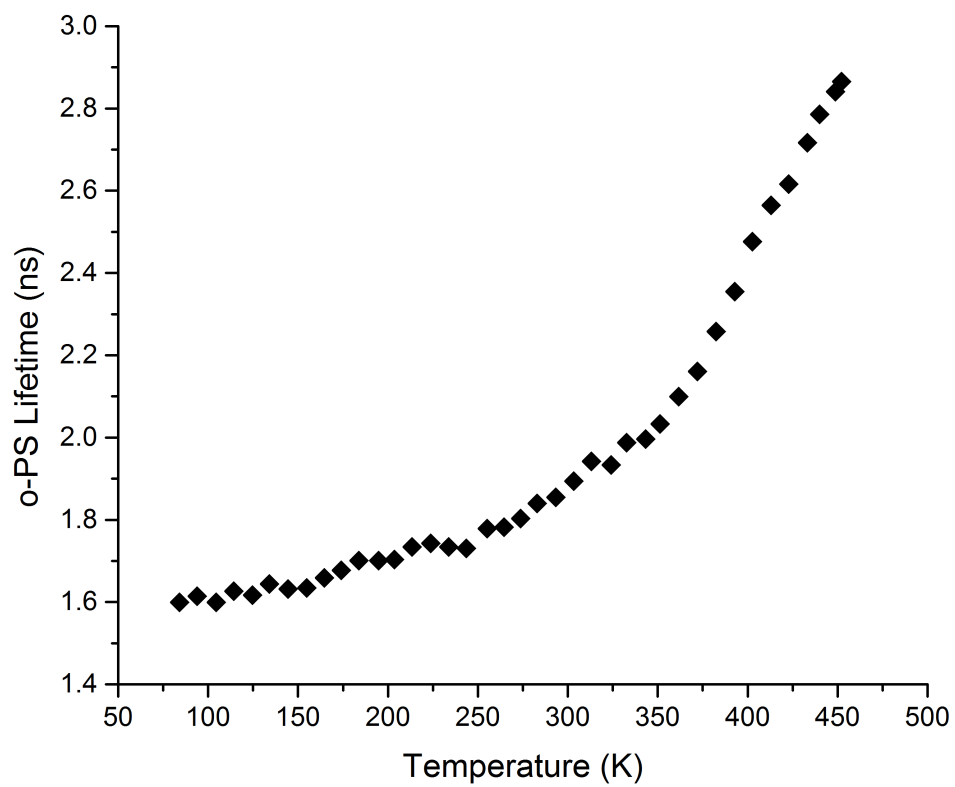


Figure S12: Temperature-dependent positron spectroscopy (PS) determined positronium lifetime of amorphous PMMA digitised from.<sup>26</sup>

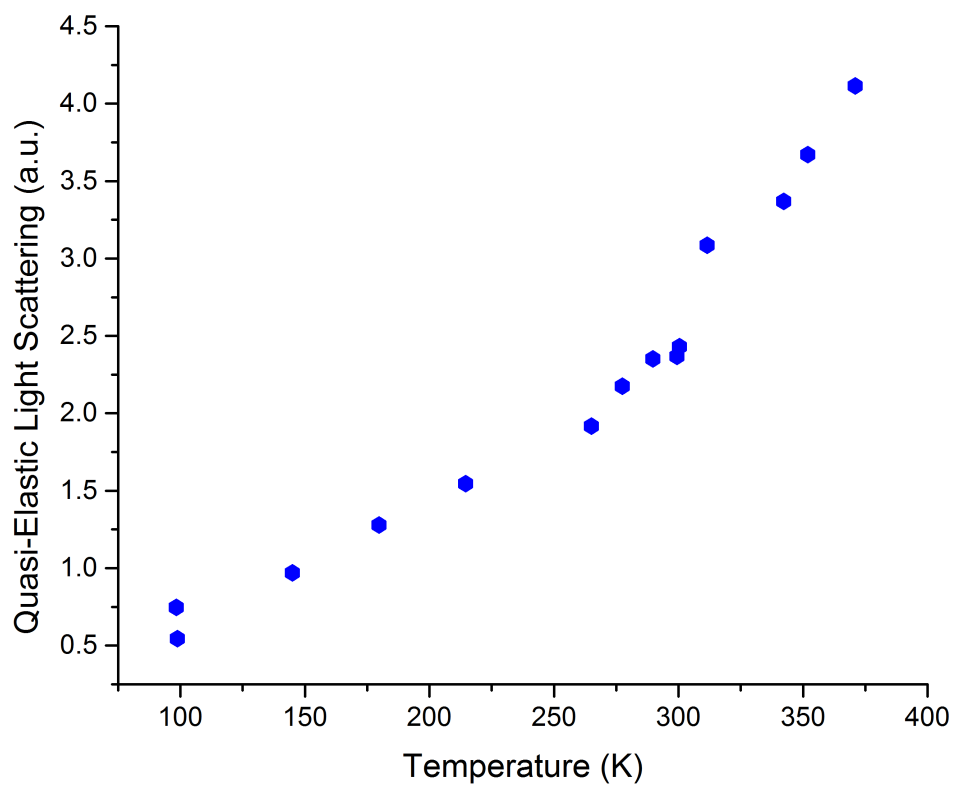


Figure S13: Temperature-dependent quasi-elastic light scattering intensity of amorphous PMMA digitised from.<sup>24</sup>

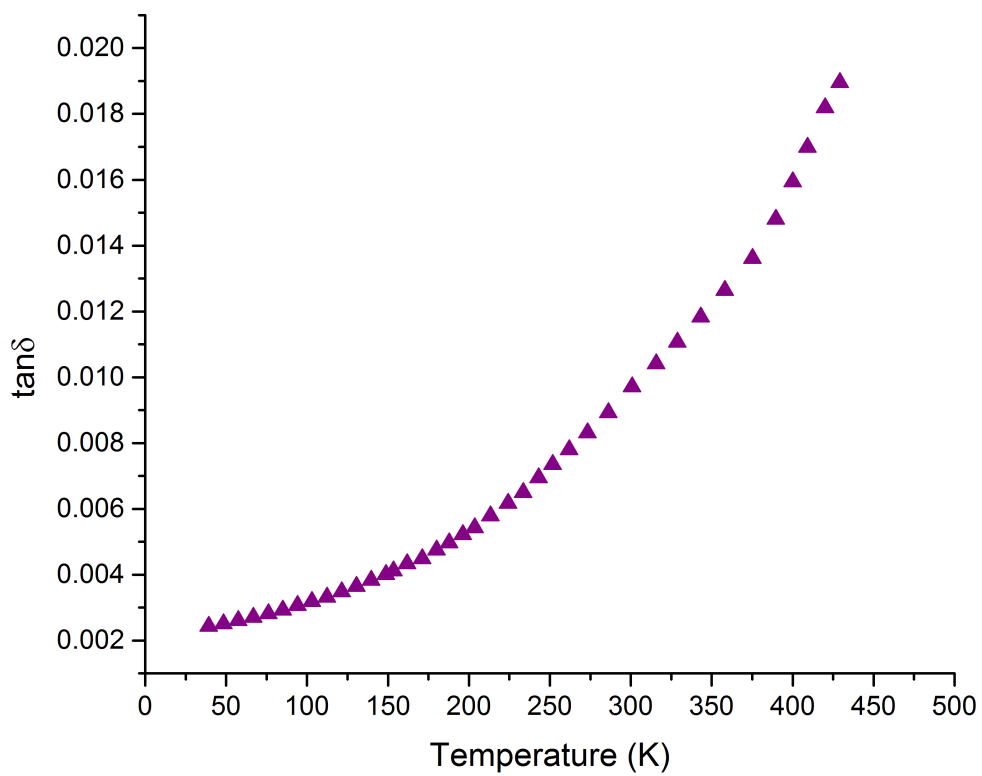


Figure S14: Temperature-dependent 10 GHz dielectric loss of amorphous PMMA digitised from.<sup>27</sup>

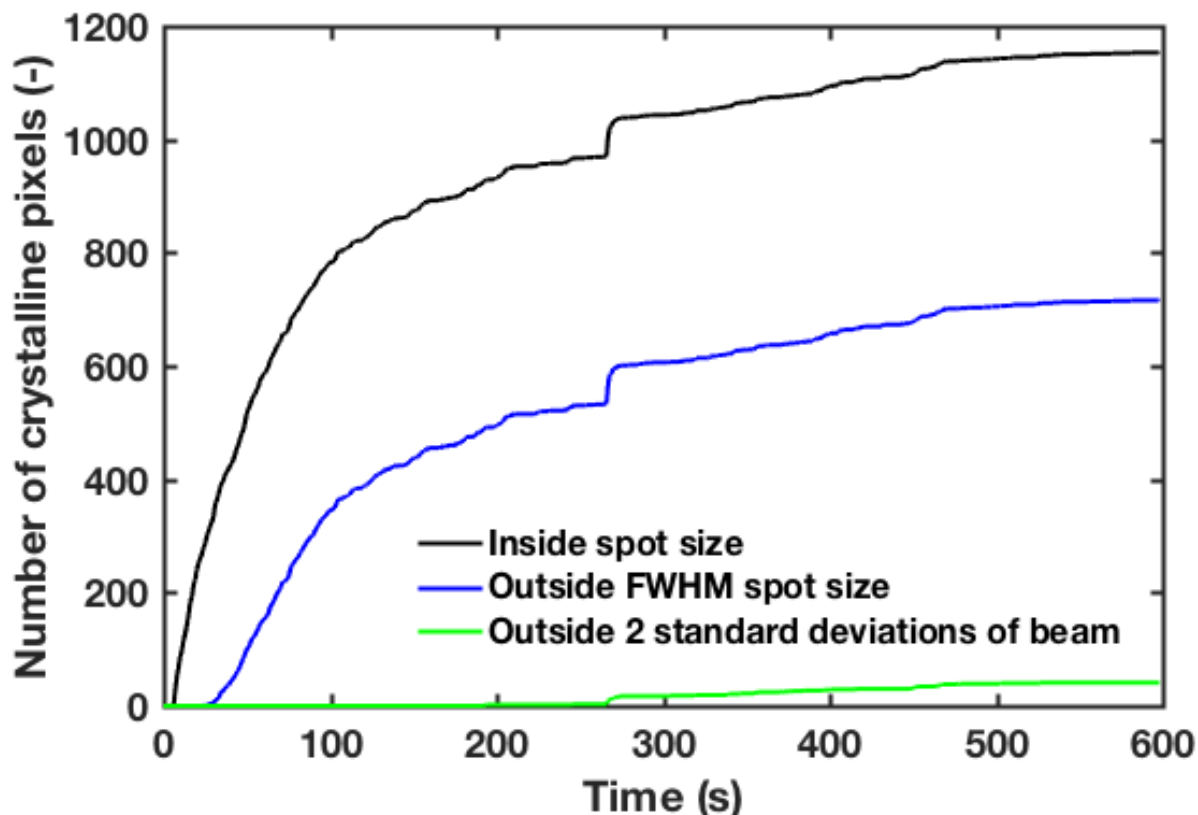


Figure S15: Time-evolution of the crystalline growth in amorphous indomethacin while exposed to FLARE. Three curves are drawn, corresponding to within the FLARE beam spot side (black), within 2 standard deviations (FWHM assuming a gaussian profile, blue). and outside of 2 standard deviations (green). The lack of any measurable change outside of 2 standard deviations of the beam spot size indicates that crystallisation was directly attributed to the high-powered THz pulses.

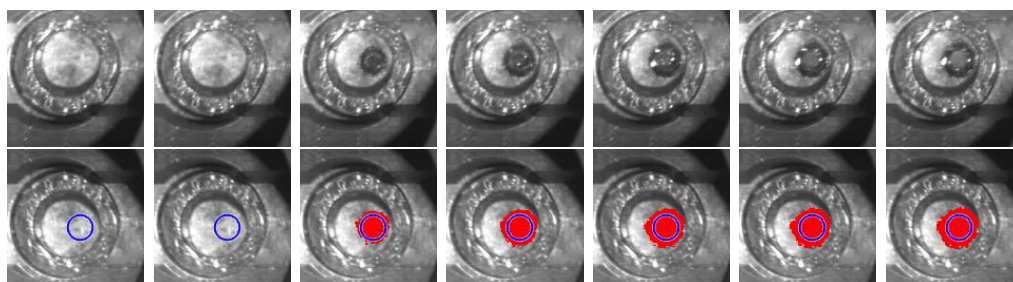


Figure S16: Video stills of the sample from Figure S15. The sample was held within a brass ring of 9 mm i.d. with the approximate position of the FLARE beam marked by the blue circle. Images are acquired at 100 s intervals (sequence from left,  $t = 0$  to right). The files of the processed and unprocessed data can be accessed in the electronic supplements (flare\_IND\_processed\_spedup.mov, video is speed up by a factor of 10).

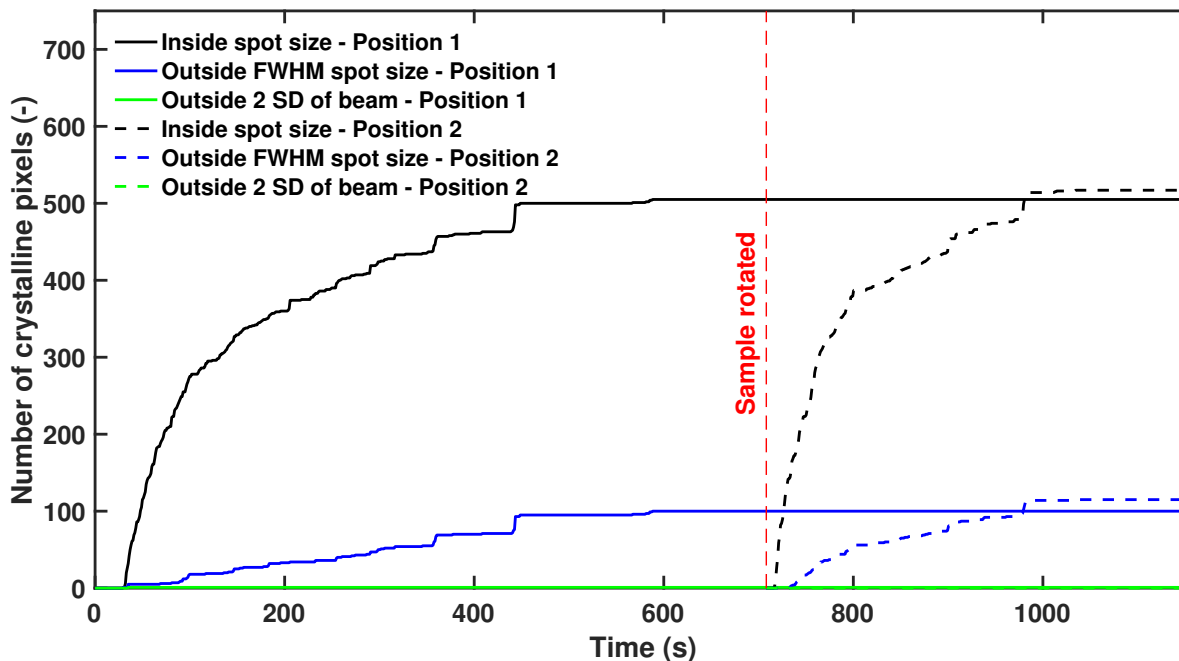
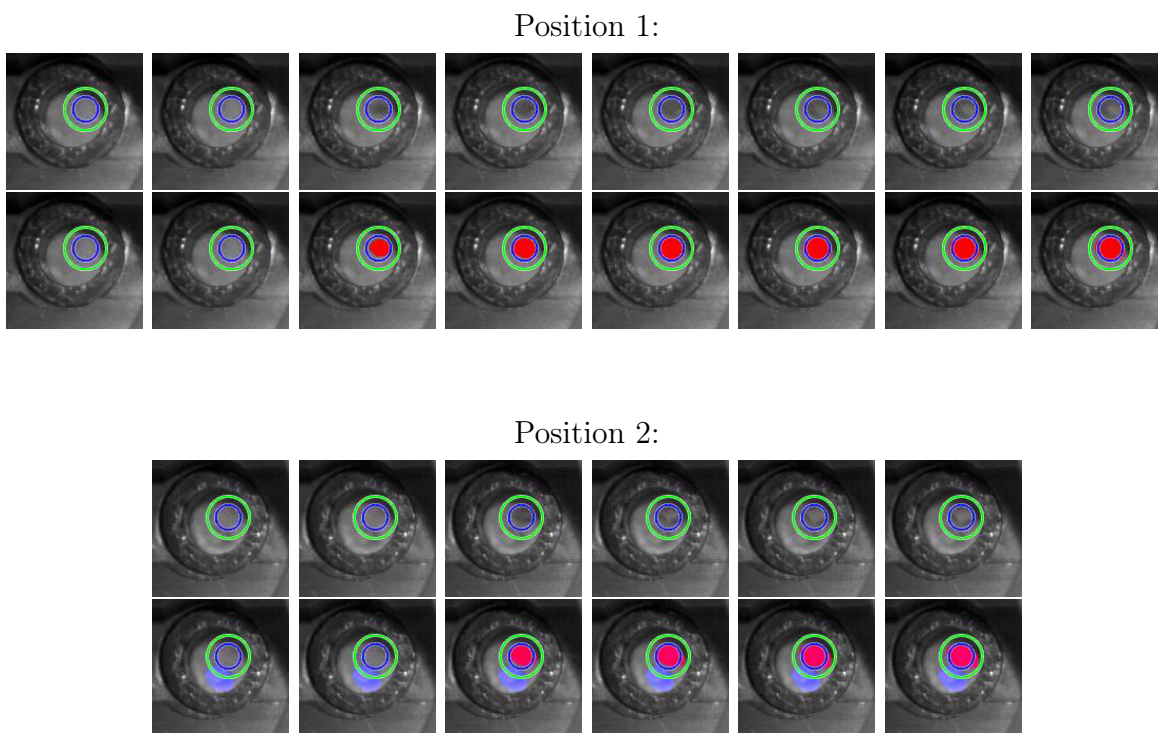


Figure S17: Time-evolution of the crystalline growth in amorphous carbamazepine while exposed to FLARE (sample kept at room temperature) after image analysis of the data shown in Fig.S18. Sample was a free-standing pellet of amorphous carbamazepine prepared by compacting freshly quench-cooled sample into a pellet of 13 mm diameter of 1.44 mm thickness. The FLARE beam (diameter of  $\approx 1.5$  mm) was focused on the sample (diameter of 13 mm) off centre. During exposure of the sample to the FLARE beam the temperature at the focal spot reached 324 K. The same sample was used for a second exposure experiment to FLARE. For the second experiment the sample was rotated after the initial exposure for 600 s so that a second area of the sample was within the FLARE beam. The data shows that in both cases crystallisation only occurs within the spatial confines of the beam spot, with the solid-line representing the first run and the dotted line representing the second. The lack of any measurable change outside of 2 standard deviations of the beam spot size indicates that crystallisation was directly attributed to the high-powered THz pulses. The slightly faster crystallisation kinetics observed during the second run on the same sample is attributed to the slightly different thermal history as well as ageing for the second experiment.



**Figure S18:** Video stills of the sample from Figure S17. The sample was held within a brass ring of 9 mm i.d. with the approximate position of the FLARE beam marked by the blue circle. Images are acquired at 100 s intervals (sequence from left,  $t = 0$  to right). The lack of any measurable change outside of 2 standard deviations of the beam spot size indicates that crystallisation was directly attributed to the high-powered THz pulses. The files of the processed and unprocessed data can be accessed in the electronic supplements (`flare_CBZ_run1_processed.mov` and `flare_CBZ_run2_processed.mov`).

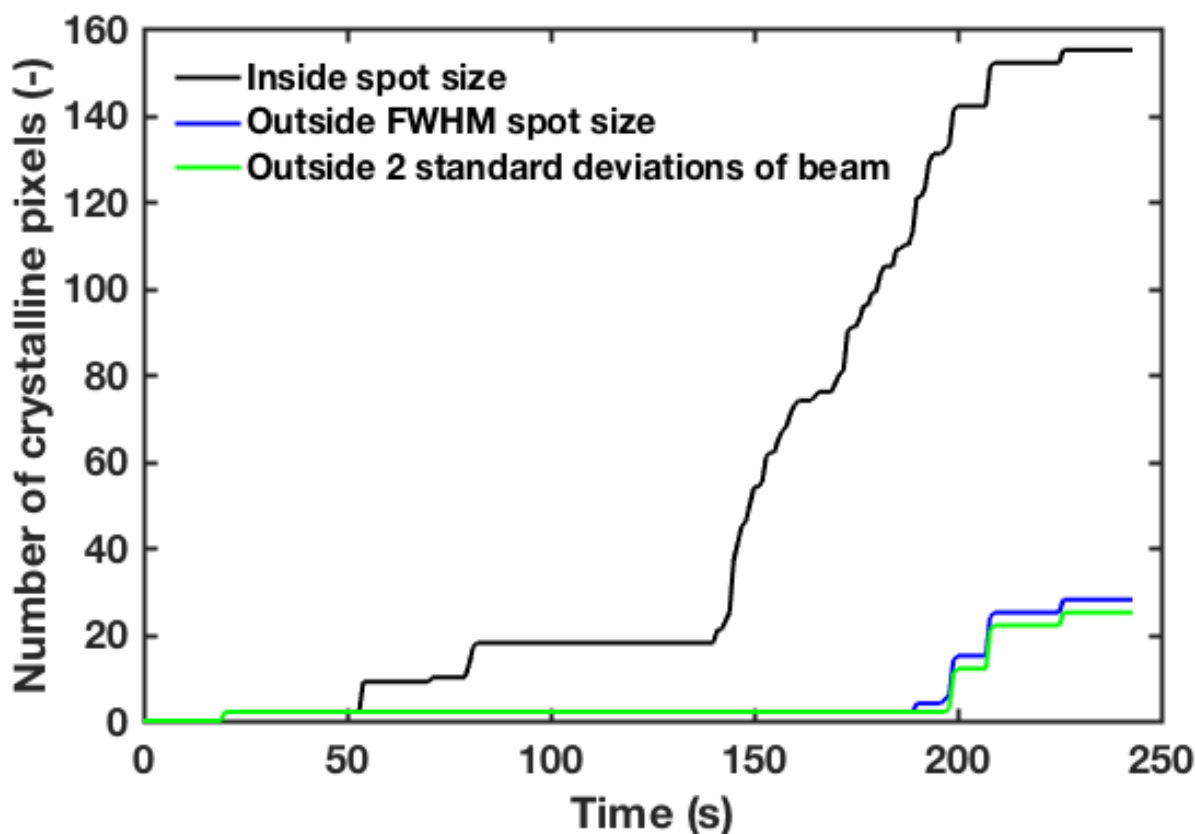
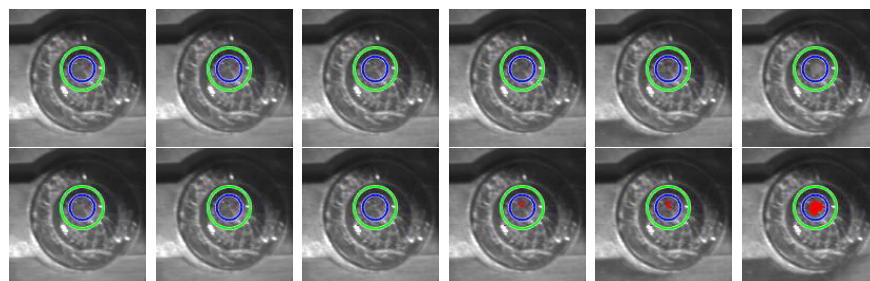
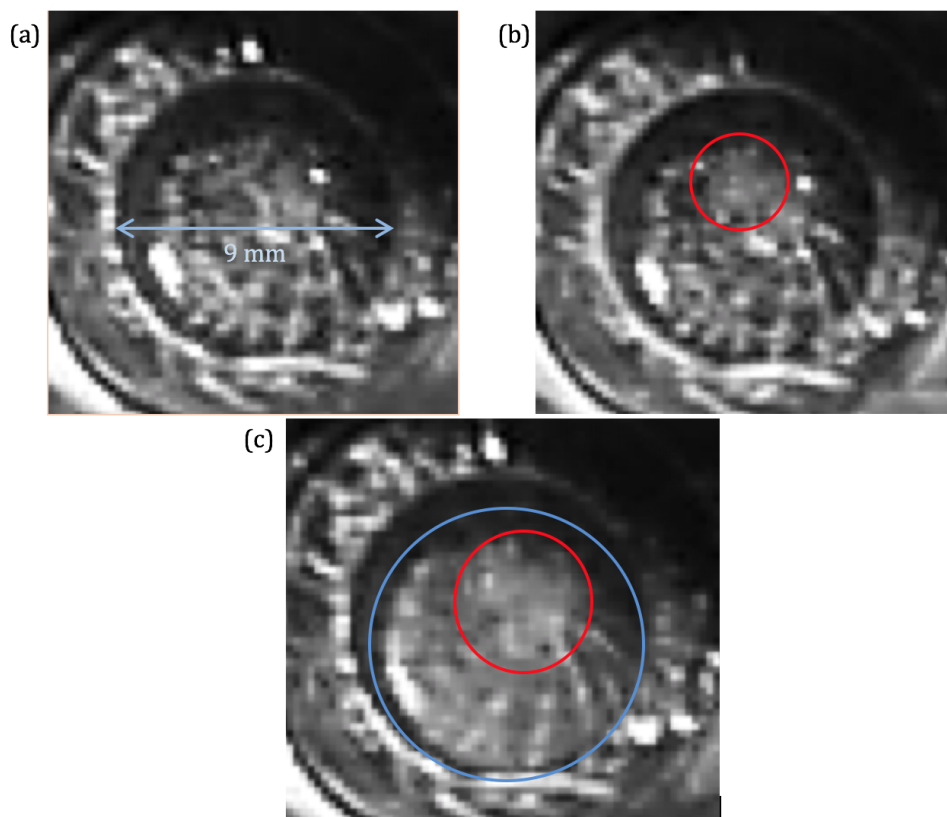


Figure S19: Time-evolution of the crystalline growth in amorphous carbamazepine following exposure to the FLARE beam under continuous liquid nitrogen flow after image analysis of the data shown in Figure S20. The sample comprised of a thin film of amorphous carbamazepine that was directly melted on a window of amorphous silica and then quench cooled. The sample was mounted on the cold finger of the open cryostat cooled to 100 K and exposed to FLARE for 100 s. Visually a small speckle at the position of the FLARE beam was discernible following FLARE illumination which was consistent with the observation of nucleation in previous experiments. The sample was heated to 263 K and a video data was acquired. The sample was heated up from 263 K at  $t = 0$  s to 293 K at  $t = 190$  s using a nominal heating rate of  $10 \text{ K min}^{-1}$ . At  $t = 190$  s the set point temperature was increased to 313 K at a heating rate of  $20 \text{ K min}^{-1}$ , which was reached at 250 s. The lack of any measurable change outside of 2 standard deviations of the beam spot size indicates that crystallisation was directly attributed to the high-powered THz pulses.



**Figure S20:** Video stills of the sample held within a brass ring of 9 mm i.d. with the approximate position of the FLARE beam marked by the blue circle. Images are acquired at 50 s intervals (sequence from left,  $t = 0$  to right). Raw images are shown at the top and the crystallisation area is highlighted in red in the bottom row following image analysis. The lack of any measurable change outside of 2 standard deviations of the beam spot size indicates that crystallisation was directly attributed to the high-powered THz pulses. The files of the processed and unprocessed data can be accessed in the electronic supplements (flare\_CBZ\_tablet1\_run1\_processed.mov).



**Figure S21:** (a) Amorphous CBZ sample 5 at 240 K, (b) CBZ sample 5 at 280 K after an initial 700 s of exposure to FLARE with crystallised region highlighted in red. It was found that a visually observable crystalline seed was produced in the region exposed to FLARE, when the recorded temperature of the region was about 280 K. Localised crystal growth is observed in this region over the next 60 s and then no further growth was seen (b). At 40 minutes and a sample temperature of 326 K, crystal growth begins to occur from the sides of the sample, eventually resulting in the crystallisation of the entire sample. (c) CBZ sample 5 after heating to 336 K, crystalline region at FLARE spot highlighted in red (CBZ form III) and bulk crystalline region (CBZ form I) highlighted in blue.

## References

- (1) Hutter, J.; VandeVondele, J.; Iannuzzi, M.; Iannuzzi, M.; Vandevondele, J.; Schiffmann, F.; Schiffmann, F.; VandeVondele, J. *WIREs Comput Mol Sci* **2014**, *4*, 15–25.
- (2) VandeVondele, J.; Krack, M.; Mohamed, F.; Parrinello, M.; Chassaing, T.; Hutter, J. *Comput. Phys. Commun.* **2005**, *167*, 103–128.
- (3) Perdew, J.; Burke, K.; Ernzerhof, M. *Phys. Rev. Lett.* **1996**, *77*, 3865–3868.
- (4) Hutter, J. V.; Jürg, J. *Chem. Phys.* **2007**, *127*, 114105.
- (5) Goedecker, S.; Teter, M.; Hutter, J. *Phys Rev B* **1996**, *54*, 1703–1710.
- (6) Grimme, S.; Ehrlich, S.; Goerigk, L. *J. Comput. Chem.* **2011**, *32*, 1456–1465.
- (7) Grimme, S.; Antony, J.; Ehrlich, S.; Krieg, H. *J. Chem. Phys.* **2010**, *132*, 154104.
- (8) Nosé, S. *J. Chem. Phys.* **1998**, *81*, 511–519.
- (9) Martyna, G. J. *Mol. Phys.* **1996**, *87*, 1117–1157.
- (10) Martyna, G. J.; Tobias, D. J.; Klein, M. L. *J. Chem. Phys* **1994**, *101*, 4177–4189.
- (11) Ruggiero, M. T.; Zeitler, J. A. *J. Phys. Chem. B* **2016**, *120*, 11733–11739.
- (12) Thomas, M.; Brehm, M.; Fligg, R.; Vöhringer, P.; Kirchner, B. *Phys Chem Chem Phys* **2013**, *15*, 6608–6622.
- (13) Brehm, M.; Kirchner, B. *J. Chem. Inf. and Model* **2011**, *51*, 2007–2023.
- (14) Kresse, G.; Furthmüller, J. *Phys. Rev. B* **1996**, *54*, 11169–11186.
- (15) Kresse, G.; Furthmüller, J. *Comp. Mat. Sci.* **1996**, *6*, 15–50.
- (16) Kresse, G.; Hafner, J. *Phys Rev B* **1994**, *49*, 14251–14269.

- (17) Kresse, G.; Hafner, J. *Phys Rev B* **1993**, *47*, 558–561.
- (18) Kresse, G.; Joubert, D. *Phys Rev B* **1999**, *59*, 1758–1775.
- (19) Monkhorst, H. J.; Pack, J. D. *Phys Rev B* **1976**, *13*, 5188–5192.
- (20) Ruta, B.; Monaco, G.; Scarponi, F.; Fioretto, D. *Philos Mag* **2008**, *88*, 3939–3946.
- (21) Bartsch, E.; Fujara, F.; Kiebel, M.; Sillescu, H.; Petry, W. *Berichte der Bunsengesellschaft für physikalische Chemie* **1989**, *93*, 1252–1259.
- (22) Monaco, G.; Caponi, S.; Di Leonardo, R.; Fioretto, D.; Ruocco, G. *Phys Rev E* **2000**, *62*, R7595–R7598.
- (23) Schnauss, W.; Fujara, F.; Sillescu, H. *J. Chem. Phys.* **1992**, *97*, 1378.
- (24) Duval, E.; Mermet, A.; Surovtsev, N.; Jal, J. F.; Dianoux, A. J. *Philosophical Magazine Part B* **2009**, *77*, 457–461.
- (25) H A Hristov,; B Bolan,; A F Yee,; Xie, L.; ; Gidley, D. W. *Macromolecules* **1996**, *29*, 8507–8516.
- (26) Qi, N.; Chen, Z. Q.; Uedono, A. *Radiat Phys Chem* **2015**, *108*, 81–86.
- (27) Amrhein, E. M.; Mueller, F. H. *Trans Faraday Soc* **1968**, *64*, 666–676.